



## Reducing high temperature corrosion when burning waste by adding digested sewage sludge

Sofia Karlsson<sup>1</sup>, Lars-Erik Åmand<sup>2</sup> and Jesper Pettersson<sup>3</sup>

<sup>1</sup>Chalmers University of Technology, Department of Chemical and Biological Engineering,  
The Swedish High Temperature Corrosion Centre, HTC,  
SE-412 96 Göteborg,  
Sverige  
Sofia.karlsson@chalmers.se

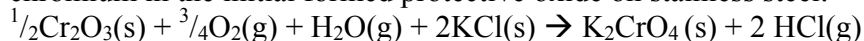
<sup>2</sup>Chalmers University of Technology, Department of Energy & Environment,  
Division of Energy and Environment  
SE-412 96 Göteborg,  
Sverige  
lars-erik.amand@chalmers.se

<sup>3</sup>Chalmers University of Technology, Department of Chemical and Biological Engineering,  
The Swedish High Temperature Corrosion Centre, HTC,  
SE-412 96 Göteborg,  
Sverige  
jpetter@chalmers.se

### ABSTRACT

The presence of alkali chlorides are well known to cause high temperature corrosion during combustion of biomass and waste. Low alloyed steels as well as stainless steels are experiencing an accelerated corrosion attack in such environments. Even though more highly alloyed steels (*i.e.* higher Cr/Fe ratio in the steel) are being used, there is only a small decrease in corrosion rate compared to low alloyed steels. To maintain the corrosion rates at an acceptable level the temperature of the superheaters (used for steam production to the steam turbine) of the boiler have been lowered. However, this causes a decrease in power production when the driving force for waste-to-energy boilers in the future is to increase the power production by increasing the temperatures of the steam from the final superheater stage.

One of the reasons for the corrosive behavior of alkali chlorides towards stainless steels is the formation of alkali chromates. It has been shown that alkali chlorides react with chromium in the initial formed protective oxide on stainless steel:



This result in a chromium depleted oxide which is converted into an iron-rich fast-growing oxide. This oxide has much poorer protective properties as it has higher diffusion rates compared to chromium rich oxides. Furthermore, the iron rich oxide is also more susceptible towards chlorine induced corrosion by chlorine ions penetrating the oxide scale. This leads to the formation of transition metal chlorides (*e.g.* FeCl<sub>2</sub>) at the metal/oxide interface causing poor scale adherence.

A way to mitigate the alkali chloride induced corrosion is by introducing fuel additives and thus, changing the flue gas chemistry and furthermore the deposit composition. In



this study, the effect of digested sewage sludge as fuel additive was investigated at the 12MW circulating fluidized bed (CFB) boiler at Chalmers University of Technology. The initial corrosion attack of the stainless steel 304L(Fe18Cr10Ni) exposed at 600°C (material temperature) was investigated during 24h exposure of three different environments. Deposit analysis by means of XRD and IC were carried out using Sanicro 28 (Fe35Cr27Ni31) as sample ring. The exposures were denoted “RDF” (a reference exposure 80%Bark + 20%RDF), “SjöMed” (80%Bark + 20%RDF with sewage sludge from Sjölundaverket (medium dosage)) and “HimHög” (80%Bark + 20%RDF with sewage sludge from Himmerfjärdsverket (high dosage)).

The results showed that the most severe corrosion attack of 304L occurred in the “RDF” exposure. The corrosion attack was characterized by an up to 100µm thick corrosion product layer and signs of internal corrosion of the steel. The deposit in the RDF exposure was dominated by alkali chlorides. The exposures with sewage sludge additions, “SjöMed” and “HimHög”, showed a remarkable decrease in corrosion rate. 304L performed especially well in the “HimHög” exposure, the steel ring was protected by a thin oxide, less than 0.3µm in thickness. Furthermore, the deposit was dominated by sulphate- and phosphate containing compounds. The presence of alkali chlorides was low.

**Keywords: alkali chloride induced corrosion, additives, digested sewage sludge**

## 1. INTRODUCTION

The production of electricity from renewable energy sources, like waste and bio fuels, is presently increasing all over the world. As these fuels are renewable, they are not considered to have any net contribution of CO<sub>2</sub> to the atmosphere when combusted. However, one drawback with these fuels is that a very aggressive flue gas is produced during combustion. Compared to fossil fuels, the alkali chloride content can be very high while the sulfur dioxide content is typically low [1]. Hence, the deposits formed on the superheater tubes are often rich in alkali chlorides (mostly KCl and NaCl) and it has been shown that high temperature corrosion of stainless steels is greatly enhanced by the presence of alkali chlorides [2]. The high corrosion rate in waste fired boilers is often explained by chlorine induced corrosion or the occurrence of low-melting heavy metal salts [3-7]. Another possibility to explain the high corrosivity of alkali chlorides is by the chromate formation mechanism [8, 9]. It has been shown that KCl and NaCl can react with the protective, chromium rich scale on 304L, forming alkali chromate[10]. The formation of alkali chromate depletes the scale in chromium which results in an iron rich, poorly protective and fast growing scale. This reaction scheme is also true for other alkali containing salts (e.g. K<sub>2</sub>CO<sub>3</sub> [11]) as well as other chromia forming steels [12]. The high temperature corrosion causes high material costs and as a consequence, the maximum steam temperature is kept considerably lower compared to fossil fuel fired plants. Hence, corrosion mitigating techniques are needed in order to reach acceptable corrosion rates with maintained or higher efficiency in the production of power in waste-to-energy boilers. One possible technique is by changing the corrosive environment in these boilers by means of fuel additives. Laboratory studies of 304L at 600°C have shown that the presence of K<sub>2</sub>SO<sub>4</sub> does not induce any accelerated corrosion attack. The non corrosive nature of K<sub>2</sub>SO<sub>4</sub> at this temperature is explained by its reluctant to react with the

protective, chromium rich oxide to form  $K_2CrO_4$ . Thus, the corrosion properties of the stainless steel remain intact. By increasing the available sulphur in the boiler, corrosive alkali chloride can be converted into the corresponding and less corrosive alkali sulphate. This can be done by using fuel additives and digested sewage sludge has earlier shown promising results in lowering the content of alkali chlorides in the flue gas and in deposits [A, B, C]. In this study, two different digested sewage sludges were tested as fuel additives at the 12MW CFB boiler at Chalmers campus. The focus is directed towards the initial corrosion attack of the stainless steel 304L and how these additives can mitigate the corrosive nature of the reference fuel (RDF and Bark). Special attention is paid to the presence of sulphur, phosphorus, calcium and aluminum silicates in the additives.

## 2. EXPERIMENTAL

### 2.1 Research boiler and operating conditions

The work presented in this paper was part of a large research program including combustion issues, ash sintering and alkali metal chemistry as well as investigations of super heater corrosion [D]. Figure 1 shows a schematic sketch of the 12 MW circulating fluidised bed (CFB) boiler located at Chalmers University of Technology.

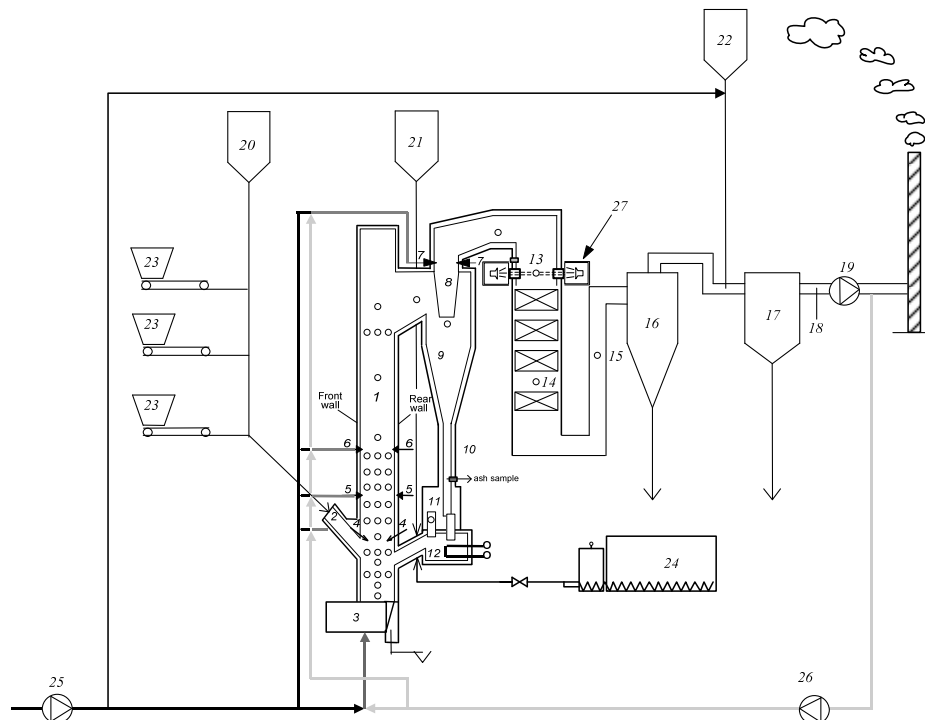


**Figure A.** Overview of the Chalmers CFB research boiler facility. (1) combustion chamber; (2) fuel feed chute; (3) air plenum; (4) secondary air inlet at 2.1m; (5) secondary air inlet at 3.7m; (6) secondary air inlet at 5.4m; (7) secondary air inlet into cyclone exit duct; (8) cyclone exit duct (9) hot primary cyclone; (10) particle return leg; (11) particle seal; (12) particle cooler; (13) measurement hole cr1; (14) measurement hole cr2; (15) measurement hole after convection pass; (16) cold secondary cyclone; (17) bag house filter; (18) gas-extraction probe for emission monitoring; (19) flue gas fan; (20) sand bin; (21) lime bin; (22) hydrated lime bin; (23) fuel bunkers; (24) sludge pump (25) air fan; (26) flue gas recirculation fan; (27) IACM instrument.



The combustion chamber (1) has a cross section of 2.25 m<sup>2</sup> and a height of 13.6 m. The various fuels are fed to the bottom of the bed through a fuel feed chute (2). The circulating material is separated at a primary cyclone (9) and returned to the combustion chamber through the cyclone leg (10) and particle seal (11). An external heat exchanger (12) cools the circulating material before re-entering the combustion chamber when required. Primary air is introduced through air nozzles located at the bottom of the riser and secondary air 2.2 m above the bottom plate (2). The exhaust gas is cooled to 150 C in the convection pass (13-14). Effective soot blowers (using steam blown probes) are installed along each section of the convection pass. These soot blowers are used regularly to keep the flue gas temperature below 180 C (once or twice every 24 h). Fly ashes are separated in the secondary cyclone (16) and the textile filter (17). Silica sand ( $d_p = 0.3$  mm) was used as bed material in all tests. The operating conditions are typical for a commercially operated CFB boiler. This means a fluidizing velocity of approx. 5 m/s in the top of the riser that leads to a proper circulation of bed material through the primary cyclone, good heat transfer of moving bed particles and an attrition of the fuel ash into fly ash, which is important in order to avoid accumulation of bottom bed ash. Typical operating conditions are also proper excess air ratio (20-25% excess air) and a bottom bed temperature of 850C

Three combustion cases were included in this work:

Case “*RDF*”: Bark pellets were co-fired with a waste (refuse derived fuel) pellets produced by IcoPower in the Netherlands. The share of waste was 22% based on the total amount of dry fuel supplied to the boiler. The bark was crushed, dried and pressed into pellets.

Case “*RDF-7%SJÖ*”: Additional combustion to the case “*RDF*” of municipal sewage sludge from a waste water treatment plant named “Sjölundaverket” with the mixture of 7.3%. “Sjölundaverket” is taking care of sewage waste water from the city of Malmö in Sweden.

Case “*RDF-13%HIM*”: Additional combustion to the case “*RDF*” of municipal sewage sludge from a waste water treatment plant named “Himmerfjärdsverket” with the mixture of 13%. “Himmerfjärdsverket” is taking care of sewage waste water from the city of Södertälje and the south-west part of Stockholm.

The element compositions of the fuels are given in Table 1. The RDF has a high chlorine content while the ash from bark and RDF have a high content of calcium (Ca) Both sludges were produced by using iron (Fe) sulphate as precipitation agent for phosphorous (P) which is reflected by the high Fe and P content. The digestion of the sludge during which methane (CH<sub>4</sub>) is produced leads to a higher ash concentration compared to undigested sludge. After digestion the sludge was mechanical dewatered by the use of high speed centrifuges lowering moisture content from 92% down to between 72-78%. Lower values of moisture are difficult to reach without the use of drying equipment. Moisture contents of 72-78% leads to low heating values in the range of 1-2MJ/kg fuel as supplied to the boiler. These low heating values requires a base load of fuel of higher heating values and the sludge could be more or less be regarded as an additive. Nevertheless, by adopting a condensation unit for the moisture in the flue gas (by cooling with district heating water) the heat used for vaporisation of the moisture of the sludge can be recovered.

**Table 1. Fuel compositions**

	Bark	RDF	Sludge "Sjö"	Sludge "Him"
Moisture %	10	5-15	78	72
Ash % dry	4.2	15	43	42
Element concentrations (% on dry fuel)				
C	52	46	30	31
H	5.8	6.2	4.3	4.5
O	37	32	17	17
S	0.03	0.2	1.7	1.4
N	0.48	0.77	3.9	3.6
Cl	0.02	0.53	0.1	0.06
Ash elements g/ kg dry ash				
K	46	11	12	11
Na	10	22	7.1	5
Al	26	48	50	48
Si	110	138	124	105
Fe	12	18	129	190
Ca	198	192	93	59
Mg	17	11	13	9.9
P	10	5.1	74	78
Ti	1	11	4.3	12
Ba	2.2	1.8	1.3	0.6
Effective heating value (H)MJ/kg				
H, dry fuel	19.5	17.9	12	13
H, raw	18.6	17.7	0.8	1.8

## 2.2 Measurement equipment

The flue gas composition was obtained by conventional instrumentation and a FTIR (Fourier Transform Infra Red spectrometry) instrument (Bomen MB100). Measurements of alkali chlorides (NaCl+KCl) were performed upstream of the convection pass (27) by an IACM (in-situ alkali chloride monitor). IACM (Figure b) have been used in previous projects at the same boiler and it is described in detail by Kassman et al. [E, F]. By using a gas extraction probe at the same position (13) it is possible to have check on the chlorine in the gas phase in the form of HCl. In position (13), an air cooled probe (Figure C) equipped with deposit rings was inserted into the flue gas channel. In order to simulate a superheater tube, it was maintained at a constant temperature of 600 °C during a period of 24 h of exposure to flue gases of 807-839 °C.

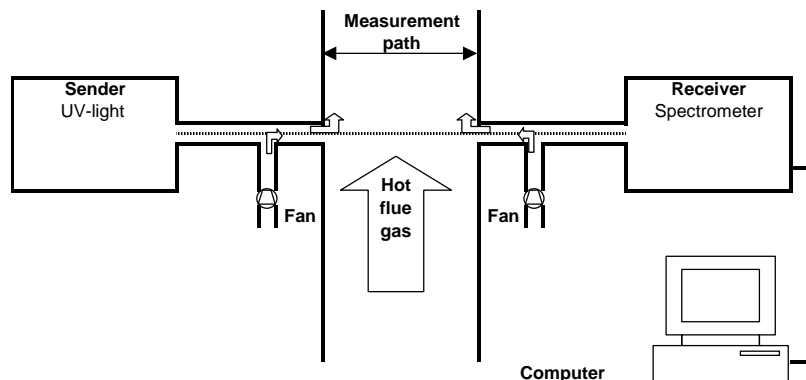


**Figure B.** Schematic view of an IACM installation

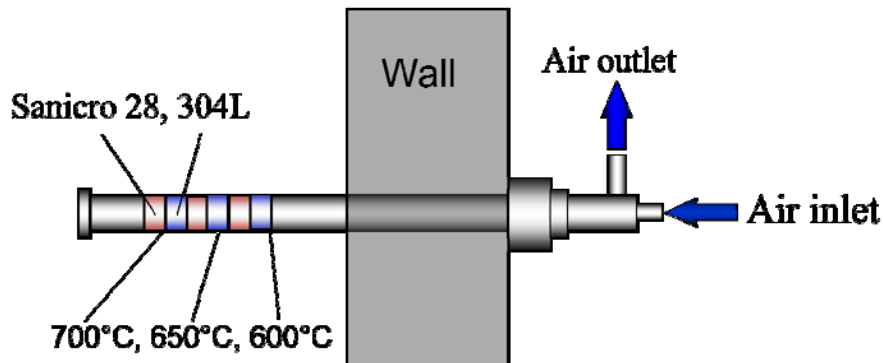


**Figure C.** The air cooled probe equipped with deposit rings at 3 different surface temperatures (700, 650, 600°C).

### 2.3 Experimental procedure

The materials used in this study are the austenitic stainless steels 304L and Sanicro 28, for chemical composition see Table 2. All samples had the form of rings with an outer diameter of 38 mm and a width of 15 mm. Before exposure the samples were degreased and cleaned in acetone and ethanol using an ultrasonic bath. The samples were dried with air and stored in plastic bottles prior to exposure. In all three different exposures (RDF, SjöMed and HimHög) two rings, 304L and Sanicro 28, were exposed for 24 hours. The temperature was kept at 600°C (material temperature). After exposure, the samples were stored dry in a desiccator. All sample rings were weight before and after exposure. The samples were also photographed after exposure.

**Table 2: Chemical composition of the alloys 304L and Sanicro 28.**

(Weight %)	Cr	Ni	Mn	Si	Mo	Fe	$n_{Cr}/n_{Fe}$	Add. elements
<b>304L</b>	19,5	9,5	1,4	1,1	0,3	67,0	0,29	-
<b>Sanicro 28</b>	27,0	31,0	<2,0	0,6	3,5	34,5	0,78	Cu: 1

### 2.4 Corrosion product characterization

In order to analyse the samples after exposure, three different analyse methods were used: SEM/EDX, XRD and IC. The 304L sample rings were mounted in epoxy and cut in order to get a cross section where deposit, oxide layer and metal could be analysed with SEM/EDX. On the Sanicro 28 sample ring, the deposit was mechanically removed in order to analyse crystalline compounds with XRD. After the XRD analysis, the deposit was leached in MQ water in order to quantify the amount of water soluble chlorine and sulphate ions.

#### 2.4.1 X-ray diffraction (XRD)

Crystalline corrosion products were analyzed by X-ray diffraction (XRD) using a Siemens D5000 powder diffractometer equipped with grazing incidence beam attachment and a Göble mirror.  $CuK_{\alpha}$  was used and the angle of incident was 2°. The detector measured between  $10^{\circ} < 2\theta < 65^{\circ}$ .

### 2.4.2 Scanning electron microscopy (SEM/EDX)

SEM imaging was performed using an FEI Quanta 200 ESEM FEG. The EDX detector was linked with the SEM and an Oxford Inca EDX system was used. The microscope was operated at 20 kV.

### 2.4.3 Ion Chromatography

To determine the amount of water soluble anions ( $\text{Cl}^-$  and  $\text{SO}_4^{2-}$ ) a Dionex ICS-90 system was used. The anions were analysed with an IonPac AS4A-SC analytic column and 1.8 mM  $\text{Na}_2\text{CO}_3/1.7\text{mM NaHCO}_3$  was used as eluent. The flow rate was 2mL/min.

## 3. RESULTS

For the three different cases “*RDF*”, “*RDF-7%SJÖ*” and “*RDF-13%HIM*” the gaseous alkali chlorides HCl and  $\text{SO}_2$  is given in Figure D. In the “*RDF*” exposure, the content of gaseous alkali chlorides (KCl+NaCl) in the flue gas was 96 ppm. By adding sewage sludge the alkali content in the flue gas decreased to 28ppm, in the “*RDF-7%SJÖ*” case and to only 3 ppm in the “*RDF-13%HIM*” case. As the alkali concentration decrease the chlorine showed up as HCl instead with an increase of HCl from 45 ppm (“*REF*” case) to 316 ppm for case “*RDF-13%HIM*”.

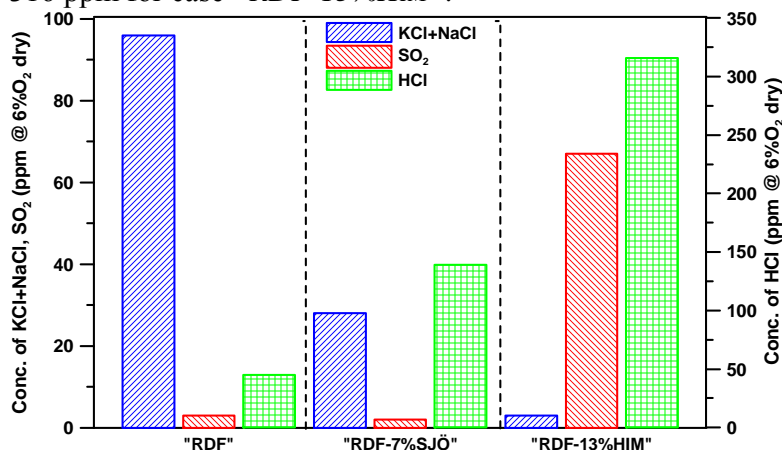


**Figure D.** Concentration of alkali chlorides (KCl+NaCl), HCl and  $\text{SO}_2$  before the convection pass (13 in Figure A) recalculated on dry flue gas at 6%  $\text{O}_2$ .

### 3.1 Optical investigation

Figure 1 shows the sample rings after 24 hours of exposure at 600°C (material temperature) in the Chalmers boiler. In the “*RDF*” case, both samples (304L and Sanicro 28) are covered by a thick, brownish deposit. The deposit layer formed on the 304L sample ring appears to be more prone towards spallation compared to the deposit formed on Sanicro 28. In the “*RDF-7%SJÖ*” case the samples are also covered by a brownish deposit layer. The deposit is dense and adherent and seems to be thinner than in the *RDF* exposure. In the “*RDF-13%HIM*” case the samples are covered by a reddish deposit. The deposit on both 304L and Sanicro 28 seems to be thinner than the deposits in the cases “*RDF*” and “*RDF-7%SJÖ*” as a metallic lustre can be seen through the deposit layer.

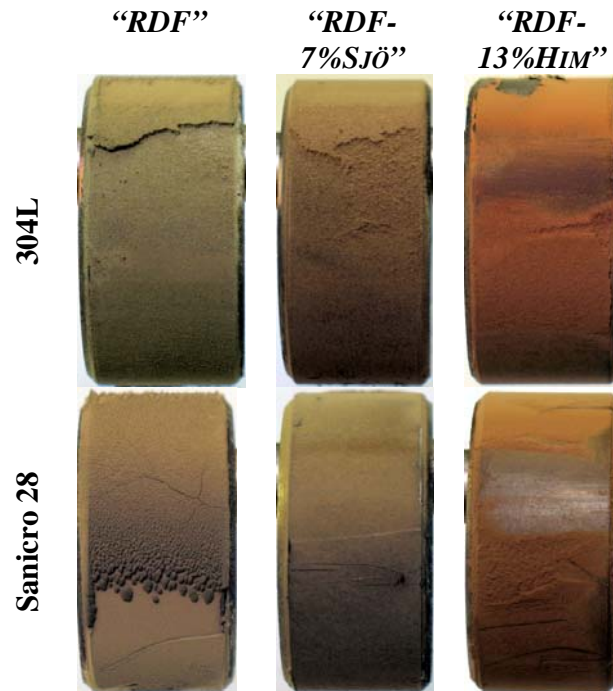


**Figure 1:** Optical images of the corrosion probe samples exposed for 24 hours at 600°C.

### 3.2 Gravimetry

All samples were weight prior to and after exposure. The mass changes are shown in Figure 2. In all exposures, Sanicro 28 and 304L experienced a mass gain, derived from the formation of deposit as well as corrosion products. However, due to the short exposure time, the mass gain is most probably dominated by the formation of deposits. Important to remember is that some of the deposits may spall off when the samples are removed from the boiler, due to large temperature variations. However, in this case, the exposure time was only 24 hours and the losses were small as the deposit layer was still rather thin and adherent.

The sample rings exposed in the “RDF” case experienced the highest mass gain. The mass gain of the Sanicro 28 ring was somewhat higher compared to the 304L sample ring. By introducing the sludge additives (*i.e.* the “RDF-7%SJÖ” and “RDF-13%HIM” cases) the mass gain decreased dramatically compared to the RDF exposure. The lowest mass gain was observed for the 304L sample in the “RDF-13%HIM” case, the mass gain being about 6 times lower compared to the “RDF” exposure. The mass gain of 304L in the SjöMed exposure is only slightly higher compared to the “RDF-13%HIM” case. Sanicro 28 shows a higher mass gain in all three exposures compared to 304L. As for 304L, the sludge additions reduced the mass gain of the Sanicro 28 ring compared to the observed mass gain in the “RDF” case. For the Sanicro 28, the lowest mass gain, more than 3 times lower compared to the “RDF” case, was observed in the “RDF-7%SJÖ” case.

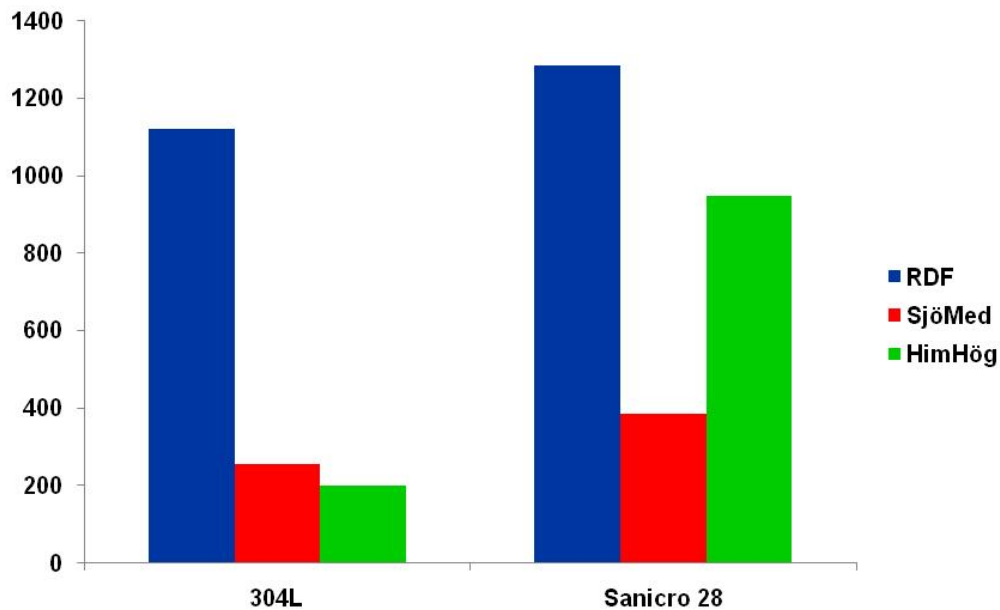


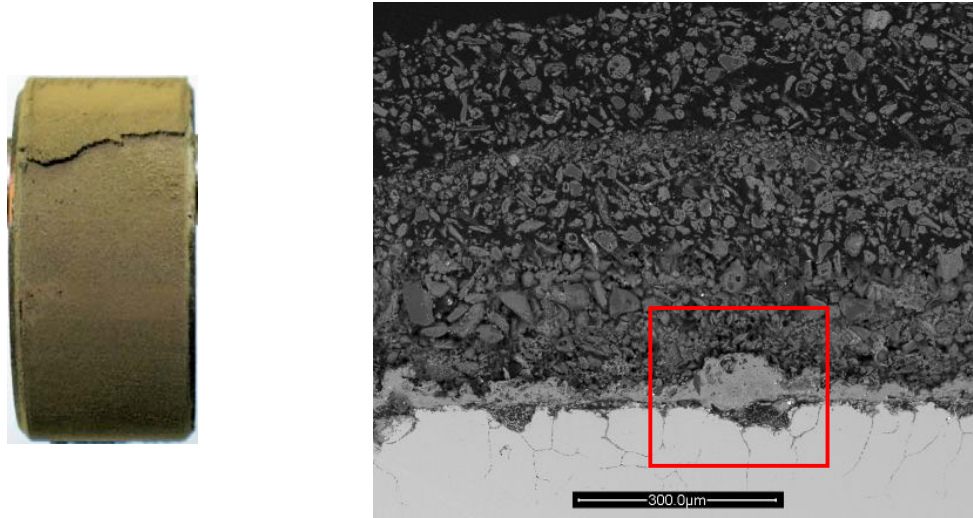
**Figure 2:** Mass change of samples made from 304L and Sanicro 28 after 24 hours of exposure at 600°C.

### 3.3 Composition of the deposit/corrosion layer by SEM/EDX

In order to investigate the deposit/corrosion layer the 304L samples were mounted in epoxy and cross sections were made. The cross sections were analyzed with SEM/EDX and are shown in section 3.3.1-3.3.3.

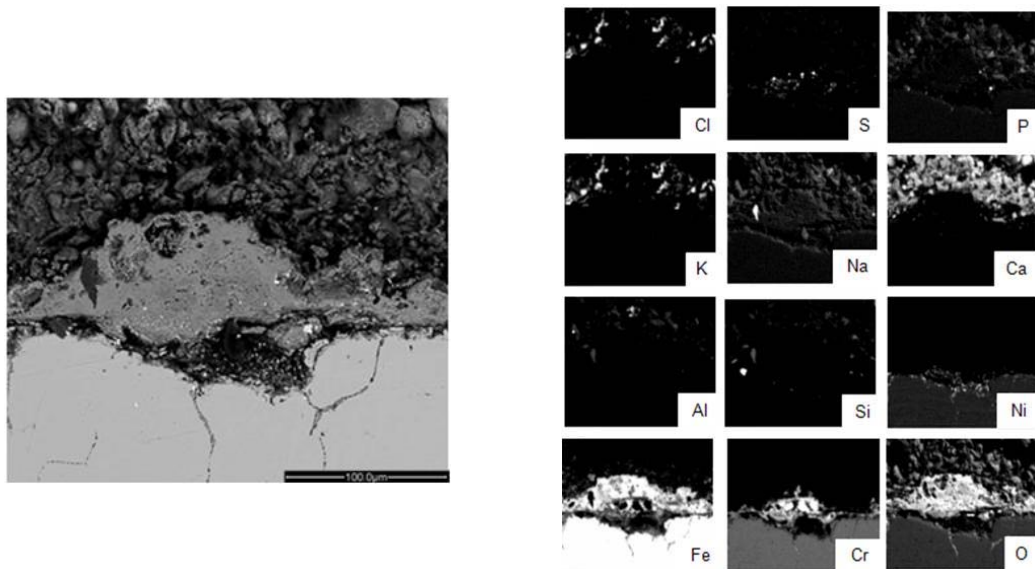
#### 3.3.1 Case “RDF” with 96 ppm alkali chlorides in the gas phase

Figure 3 shows the 304L ring exposed at 600°C for 24 hours in the “RDF” case (to the left) and a SEM image of the cross section of the corresponding sample (to the right). In the SEM image, 4 distinctive areas can be identified; the bright area in the bottom part of the image shows the steel sample ring, on top of which a rather bright corrosion product layer has formed, covered by a greyish deposit layer, casted in epoxy (black area in left top corner of the image). The thickness of the oxide layer varies and is between 30 µm to 100µm and the thickness of the covering deposit layer is 550 µm to 600µm.



**Figure 3:** (left) Optical image of 304L exposed at 600°C for 24 hours in the case “RDF” and (right) SEM image of the corresponding metallographic cross section.

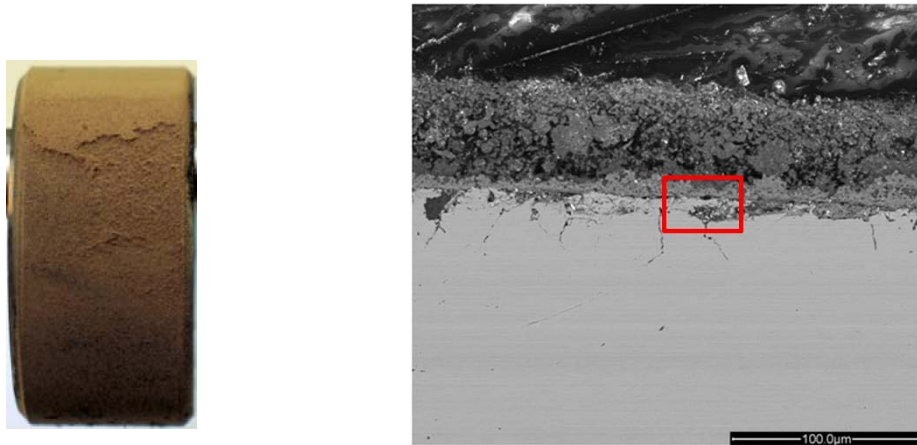
Figure 4 shows a close up image of the area marked in Figure 3. In this high magnification image, EDX analysis was performed. According to the Fe, Cr and O maps, the oxide layer can be divided into two parts. The outer part is dominated by Fe and is probably outward growing. In addition, nodules of almost pure chromia ( $\text{Cr}_2\text{O}_3$ ) could be seen embedded in the outward growing iron rich oxide. The inner part of the oxide layer contains both Fe and Cr, probably present as an inward growing oxide. In comparison to the outward growing oxide, the inward growing oxide is much thinner. Furthermore, a high void concentration can be seen in the inner part of the oxide scale as well as internal oxidation along the steel grain boundaries. The EDX analysis also shows the inner part of the deposit, which is dominated by K, Cl and Ca. In addition, small amounts of P, Na, Si



**Figure 4:** SEM image and EDX maps of the corrosion front of 304L exposed at 600°C for 24 hours in the case “RDF”. and Al is detected in the deposit layer.

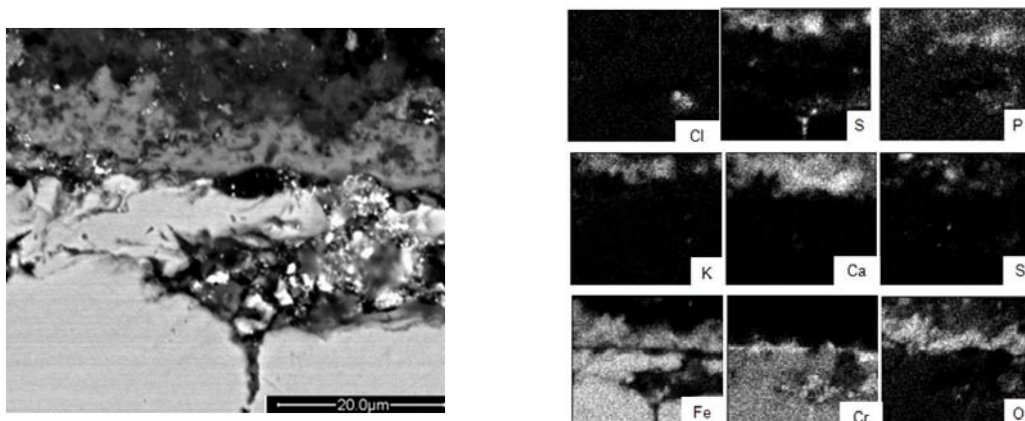
### 3.3.2 Case “RDF-7%SJÖ” with 28 ppm alkali chlorides in the gas phase

Figure 5 shows the 304L ring after 24 hours of exposure at 600°C in the case “RDF-7%SJÖ”. The cross section reveals that a 12-20µm thick oxide layer has formed. In similarity to the oxide layer formed in the “RDF” case, the scale could be divided into two parts. The outer part is quite dense and homogeneous while the inner part is more heterogeneous and voids can be seen in some areas. The sample ring also shows signs of internal oxidation along the steel grain boundaries.



**Figure 5:** (left) Optical image of 304L exposed at 600°C for 24 hours in the case “RDF-7%SJÖ” and (right) SEM image of the corresponding metallographic cross section.

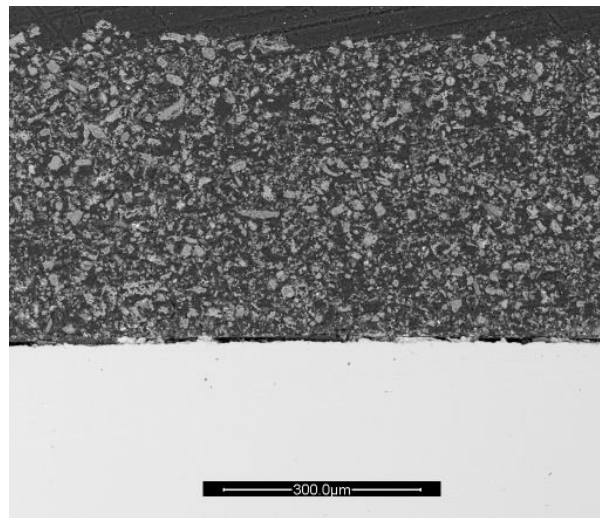
Figure 6 shows the SEM/EDX analysis of the marked area in Figure 5. The corrosion front consists of a duplex oxide scale where the outer part is Fe rich and the inner part is Cr rich. The outer, outward growing, part is roughly 4 times thicker compared to the inner, inward growing, part. The chromium rich inner part is not continuous and the chromium content is as lowest closest to the void. Some chlorine and sulphur enrichment is detected within the void. Especially sulphur can be seen decorating the lower part of the void and the steel grain boundary. Furthermore, the deposit part is dominated by K, Ca, S and P.



**Figure 6:** SEM image and EDX maps of the corrosion front of 304L exposed at 600°C for 24 hours during the case “RDF-7%SJÖ”.

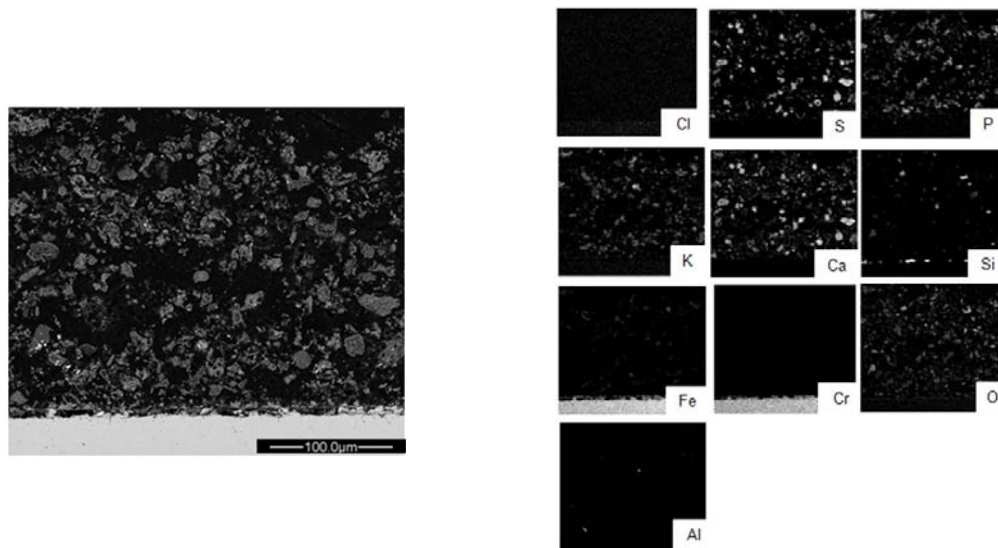
### 3.3.3 Case “*RDF-13%HIM*” with 3 ppm alkali chlorides in the gas phase

Figure 7 shows the 304L ring after 24 hours of exposure at 600°C during the case “*RDF-13%HIM*”. Unlike the deposits formed during the “*RDF*” and “*RDF-7%Sjö*” cases, the deposit formed in the *RDF-13%HIM* case is clearly red in colour. The SEM image of the cross section in Figure 7 shows the sample ring covered with deposit particles. The deposit layer consists of a porous network of individual particles, 10-50µm in size. Beneath the deposit layer, no corrosion product layer can be seen in the SEM image. Thus, the oxide formed on 304L in the “*RDF-13%HIM*” case is in the submicron range, probably less than 0.3µm in thickness. Furthermore, there are no signs of internal oxidation of the steel.



**Figure 7:** (left) Optical image of 304L exposed at 600°C for 24 hours during the case “*RDF-13%HIM*” and (right) SEM image of the corresponding metallographic cross section.

Figure 8 shows a SEM/EDX analysis of an area with higher magnification compared to the SEM image in Figure 7. The presence of a ultra-thin oxide is confirmed by the oxygen EDX map; no enrichment of oxygen can be detected on top of the steel substrate as the lateral resolution of the EDX analysis is too poor. Thus, the oxide thickness is less than 0.3µm. The deposit composition is according to the EDX analysis dominated by particles consisting of K, Ca, P and O and particles consisting of Ca, S, and O and in some occasions Ca, S, O and K.



**Figure 8:** SEM image and EDX maps of the corrosion front of 304L exposed at 600°C for 24 hours during the “RDF-13%HIM” case.

### 3.4 Deposit analysis with XRD and IC

The XRD and IC analyses were performed on the deposit/corrosion product layer formed on the Sanicro 28 rings and the results are summarized in Table 1 (XRD) and Figure 9 (IC). According to XRD strong signal from KCl and NaCl was detected in the “RDF” case. This is in agreement with SEM/EDX (Figure 4) where correlations between K and Cl can be seen in the deposits. Figure 4 also shows the outer part of the oxide is dominated by Fe which also is in agreement with the XRD analysis where Fe<sub>2</sub>O<sub>3</sub> was detected. Furthermore, weak signals from CaSO<sub>4</sub> were detected which indicates a low amount of sulphates in the deposits.

The “RDF-7%SJÖ” case also showed strong signal from KCl and NaCl. However, unlike the “RDF” case, strong signal from K<sub>2</sub>Ca<sub>2</sub>(SO<sub>4</sub>)<sub>3</sub> and CaSO<sub>4</sub> was detected. This is in agreement with the SEM/EDX results, Figure 6, where the deposits were dominated by K, Ca and S. Furthermore, medium signal from Fe<sub>2</sub>O<sub>3</sub> and SiO<sub>2</sub> was detected.

In the “RDF-13%HIM” case, no signal from alkali chlorides was detected. Instead, K<sub>2</sub>Ca<sub>2</sub>(SO<sub>4</sub>)<sub>3</sub> and CaSO<sub>4</sub> could be detected and can be seen in particles that build up the deposits in the SEM/EDX analysis, Figure 8. Furthermore, Fe<sub>2</sub>O<sub>3</sub> was detected by XRD and according to the Fe EDX map, iron is present in discrete particles throughout the whole deposit layer.

**Table 1: Crystalline compounds detected by XRD on deposits from Sanicro 28 after 24 hours of exposure at 600°C**

case/compounds	KCl	NaCl	K <sub>2</sub> Ca <sub>2</sub> (SO <sub>4</sub> ) <sub>3</sub>	CaSO <sub>4</sub>	SiO <sub>2</sub>	Fe <sub>2</sub> O <sub>3</sub>
“RDF” 600°C	S	S		W		W
“RDF-7% <i>Sjö</i> ” 600°C	S	S	S	S	M	M
“RDF- 13% <i>Him</i> ” 600°C			M	S	M	M

S = strong signal, M = medium signal och W = weak signal

The IC results in Figure 9 show a diagram of the distribution of chloride ions and sulphate ions in the deposits. It also shows the amount of ions ( $\mu\text{mol}$ ) in each case. The results show that the “RDF” case produces a deposited rich in chloride were more 95% ( $864\mu\text{mol}$ ) is dominated by chloride ions and less than 5% ( $31\mu\text{mol}$ ) was sulphate which gives a Cl/S molar ratio of 27.8. The addition of sewage sludge in the “RDF-7%*Sjö*” case resulted in deposits with roughly equal amounts of sulphate and chlorine. The Cl/S ratio in this deposit is 0.96 and the amount of chlorine ion was  $255\mu\text{mol}$  and the amount of sulphate ions  $265\mu\text{mol}$ . The addition of sewage sludge in case “RDF-13%*Him*” decreased the amounts of chlorine in the deposits to a level near the detection limit. The Cl/S ratio in this deposit layer was only 0.008 (compared to 27.8 in the “RDF” case).

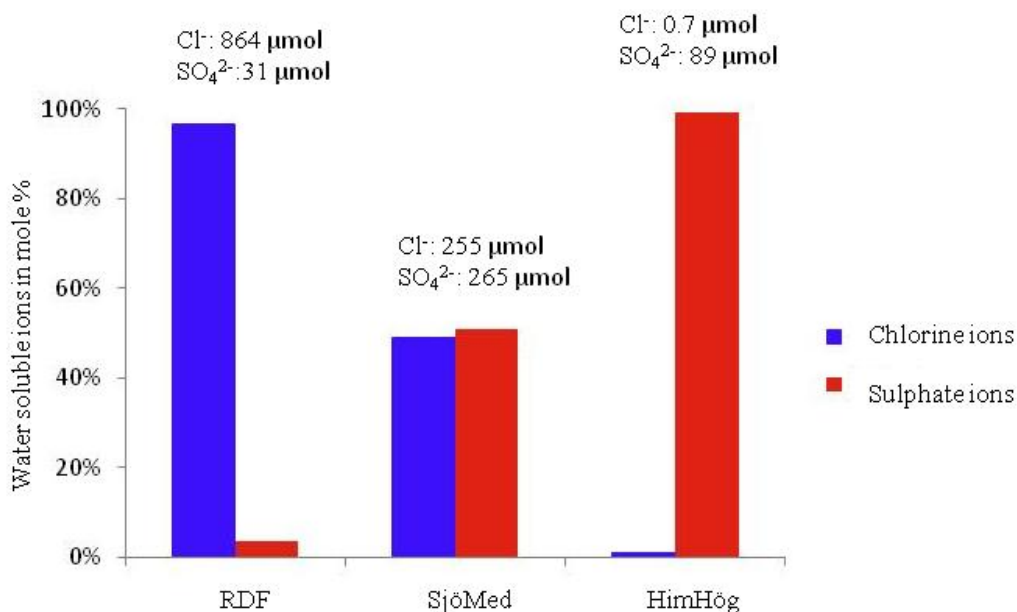


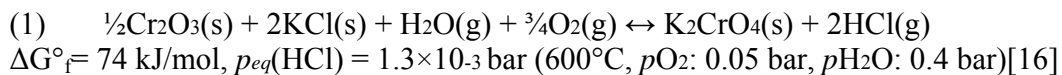
**Figure 9:** Mole% of water soluble chlorides and sulphates on the Sanicro 28 sample ring after 24 hours exposure at 600°C. The values above the bars correspond to the total amount of ions detected in the IC analysis.



## 4. Discussion

The aim of this study was to investigate what effect two digested sewage sludges used as additives had on the corrosion attack in a harsh environment created by co-combustion of RDF with bark pellets. In the reference exposure, denoted “RDF”, the fuel composition was a mixture of 78%Bark and 22%RDF calculated on dry fuel supplied to the boiler. The “RDF” case rendered in a flue gas containing high levels of gaseous alkali chlorides (96ppm), measureable levels of HCl(g) and a low level of SO<sub>2</sub>(g), Figure D. Accordingly, the deposit formed on the simulated superheater tubes, *i.e.* the corrosion probe, was dominated by alkali chlorides, mainly KCl. Moreover, the amount of deposit and corrosion products was more than 6 times higher for the samples exposed during the case “RDF” compared to the cases with additives (see Figure 2). From the IC results, the Cl/S ratio in the deposits was calculated to be 27.8.

The alkali chloride rich deposit in the “RDF” case gave rise to a very severe corrosion attack (Figure 3 and Figure 4). The corrosion attack is characterized by an oxide scale 30-100µm thick as well as internal oxidation along the steel grain boundaries and large void formation in the metal/oxide interface. The steel used for corrosion evaluation in this study is an austenitic stainless steel with 20 wt% Cr and 10 wt% Ni. In environments created by the combustion of biomass low in alkali and chlorine such as wood chips originating from stem wood, this type of steel material withstand high temperature corrosion as it forms a protective oxide consisting of a chromium rich solid solution (Cr,Fe)<sub>2</sub>O<sub>3</sub>. The oxide properties critically depend on composition, a chromia-rich oxide being protective while an iron-rich oxide (*e.g.* pure Fe<sub>2</sub>O<sub>3</sub>, hematite) is poorly protective. Hence, all reactions that deplete the oxide in chromia are potentially harmful. Previous studies in laboratory environments have shown that both H<sub>2</sub>O and KCl are active in such chromia depleting reactions [13-15]. In [14] it was shown that KCl reacts with the protective oxide formed initially on 304L, forming potassium chromate according to reaction (1):



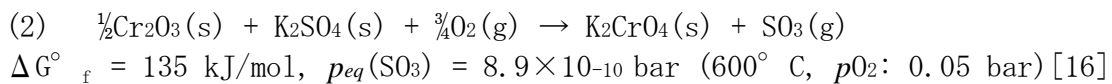
The reaction depletes the oxide in chromium and a duplex scale will form. The scale consists of an outer hematite layer and an underlying (Fe,Cr,Ni) spinel type oxide [17]. This scale is poorly protective and the corrosion attack may further be accelerated by the inward diffusion *e.g.* chloride and sulphide ions. These ions are expected to increase the diffusion rate through the corrosion product layer by decorating oxide grain boundaries [18]. In addition, metal chlorides and metal sulphides that forms in the metal/oxide interface are expected to decrease the scale adherence which in turn can lead to that sound metal is exposed for the corrosive flue gases such as HCl and SO<sub>2</sub>.

According to the EDX maps (Figure 4) and XRD (Table 1), no alkali chromate was detected which should be expected according reaction (1). However, in the chromium map nodules of pure chromium oxide can be seen in the outward growing oxide. As 304L forms a solid solution oxide of iron and chromium when oxidized, this pure chromia is not expected to have formed from oxidation of the steel. Instead, the nodules of pure



chromium oxide are probably a result of decomposition of alkali chromate. The initially formed alkali chromate, formed on the oxide surface is suggested to decompose to chromium oxide and alkali hydroxide in reducing environments. Nevertheless, chromium has been depleted from the protective oxide initially formed and the chromia nodules are not expected to be protective. Thus, the protective oxide was transformed into a poorly protective and fast growing  $\text{Fe}_2\text{O}_3$  oxide (detected with XRD, Table 1). Because of this poor protection, the underlying metal can be attacked and internal oxidation can be clearly seen in Figure 4.

On the basis of the results presented above, the corrosion attack could be mitigated by minimizing the presence of reactive alkali compounds, *e.g.* alkali chlorides. As a consequence, the protective oxide initially formed on stainless steels would remain intact and thus, the corrosion protection of the steel maintained. It has been shown in laboratory exposures that potassium in the form  $\text{K}_2\text{SO}_4$  is not aggressive towards 304L at  $600^\circ\text{C}$  in an  $\text{O}_2 + \text{H}_2\text{O}$  atmosphere [11]. The stipulated explanation is that  $\text{K}_2\text{SO}_4$  does not react with the chromium rich oxide. Hence, reaction (2) is not thermodynamically favored:



All reactions where alkali chlorides are converted into less aggressive compounds are beneficial from a corrosion point of view. Digested sewage sludge contains high levels of sulphur, phosphorus and aluminosilicates, all with the ability to react with alkali chlorides. Hence, the question is to what extent the alkali chlorides are converted by the addition of sewage sludge and secondly, is the conversion dominated by one of these species or are all three at play?

In the “REF-13%HIM” case, the effect of adding digested sewage sludge on the high temperature corrosion of 304L was remarkable. The thickness of the corrosion product layer after 24 hours of exposure at  $600^\circ\text{C}$  was less than  $0.3\mu\text{m}$ , compared to  $30\text{-}100\mu\text{m}$  in the “RDF” case. Furthermore, no signs of internal oxidation of 304L were detected in the “REF-13%HIM” case. The thin oxide formed protected the steel from corrosion and thus, it is expected to be chromium rich. However, due to the small thickness of the oxide, EDX analysis was not possible. Nevertheless, the deposit formed on the 304L sample rings in the “REF-13%HIM” case did not induce any corrosion during the 24 hours of exposure. According to the IACM results, the addition of digested sewage sludge in the “REF-13%HIM” case reduced the amount of gaseous alkali chlorides in the flue gas from 96 ppm (RDF) to 3 ppm. The decreased levels of alkali chlorides in the flue gas had a positive effect on the deposit formation. The amount of deposit decreased 6 times compared to the “RDF” case and the amount of chlorine in the deposits was almost zero, see Figure 9. Furthermore, the composition of the deposits changed radically. According to the IC analysis (see Figure 9), the presence of chloride containing compounds were near the detection limit and the Cl/S ratio was calculated to only 0.008. This was in line with the XRD analysis where only diffraction from  $\text{K}_2\text{Ca}_2(\text{SO}_4)_3$  and  $\text{CaSO}_4$  were detected. The presence of alkali and alkali earth sulphates were also detected in the SEM/EDX analysis. In addition, a correlation between K, Ca, P and O could be seen

which indicates the presence of a mixed phosphate. The presence of Al and Si in the deposit analysis was rather low. Hence, the addition of digested sewage sludge is suggested to decrease the presence of alkali chlorides mainly by sulphation but also by reacting with phosphorous and aluminium silicates in the gas phase.

In the “REF-7%SJÖ” case, the effect of digested sewage sludge was not as remarkable as in the “REF-13%HIM” case. However, the amount added sludge was less in the “REF-7%SJÖ” case compared to the “REF-13%HIM” case. In the “REF-7%SJÖ” case the gaseous alkali chlorides decreased, from 96ppm in the “RDF” case, to 28 ppm. The analysis of the deposits formed in this case detected the presence of alkali chlorides and consequently, the addition of digested sewage sludge was not high enough to convert all alkali chlorides into to more stable alkali compounds. However, compared to the “RDF” case the Cl/S decreased from 27.8 to 0.96. In addition, the deposits contained phosphorus according to the EDX analysis. The extent of the corrosion attack decreased as well; the oxide scale is thinner and more even compared to the corresponding exposure in the “RDF” case, see Figure 5. Internal oxidation of the steel did also decrease somewhat in the “REF-7%SJÖ”. However, in the areas with a higher corrosion rate, chlorine and sulphur were detected.

## 5. CONCLUSIONS

- The addition of digestive sewage sludge to the 12-MW<sub>th</sub> CFB boiler at Chalmers University of Technology resulted in a decreased corrosion rate of 304L and Sanicro 28 at 600°C after 24 hours of exposure. Without additives a thick oxide scale was formed on the samples, covered by a deposit were high amount of corrosive alkali chlorides were detected.
- The corrosivity of alkali chlorides is attributed to the formation of alkali chromate, formed by the reaction between the protective oxide and the alkali chlorides in the deposit. This results in a poorly protective and fast growing iron rich oxide.
- Adding digested sewage sludge to the fuel changes the composition of the deposit and the corrosion rate is significantly decreased. The main reason for this is that alkali chlorides in the deposit are largely being replaced by less corrosive alkali sulphates and alkali phosphates. In contrast to alkali chlorides, they do not deplete the protective oxide in chromium by forming K<sub>2</sub>CrO<sub>4</sub>. Additionally, less chlorine in the deposit decreases the possibility of formation of transition metal chlorides.

## 6. ACKNOWLEDGEMENTS

This project was financed by Värmeforsk AB (project: A08-817) and by the Swedish Energy Administration. The work was carried out within the High Temperature Corrosion Centre (HTC) together with Energy Conversion, both at Chalmers University of Technology. The practical support from the operator at Akademiska Hus AB and the research engineers employed by Chalmers University of Technology is also greatly appreciated.



## 7. REFERENCES

- A. Åmand, L.-E., Leckner, B., Eskilsson, D., Tullin, C. *Deposits on heat transfer tubes during co-combustion of biofuels and sewage sludge*, Fuel, vol. 85, pp. 1313-1322, 2006.
- B. Davidsson, K.O., Åmand L.-E., Elled, A.-L., Leckner, B. *Effect of co-firing coal and biofuel with sewage sludge on alkali problems in a circulating fluidized bed boiler*, Energy and Fuels, vol. 21, pp. 3180-3188, 2007.
- C. Elled, A.-L., Davidsson, K.O., Åmand, L.E., *Sewage sludge as a deposit inhibitor when co-fired with high potassium fuels*, Biomass and Bioenergy, vol. 34, pp. 1546-1554, 2010.
- D. S. Herstad Svärd, B-M. Steenari, L-E. Åmand, J. Bowalli, J. Öhlin, J. Pettersson, S. Karlsson, E. Larsson, J-E. Svensson, L-G. Johansson, K. Davidsson, L. Bäfver, M. Almark, *Measures for simultaneous minimization of alkali related operating problems, Phase 3*, Värmeforsk Report Project A08-817, 2010.
- E. H. Kassman, L. Bäfver, L. E. Åmand, *The importance of SO<sub>2</sub> and SO<sub>3</sub> for sulphation of gaseous KCl – An experimental investigation in a biomass fired CFB boiler*, Combust. Flame vol. 157, pp. 1649-1657, 2010.
- F. H. Kassman, J. Bohwalli, J. Pettersson, L.-E. Åmand, *Ammonium Sulphate and Co-Combustion with Peat - Two Strategies to Reduce Gaseous KCl and Chlorine in Deposits during Biomass Combustion*, Impact of Fuel Quality, Saariselkä, Finland, 2010.
1. Pettersson, J., Pettersson, C., Folkesson, N., Johansson, L.-G., Skog, E. and Svensson, J.-E., *The influence of sulphur additions on the corrosive environment in a waste-fired CFB boiler*. Materials Science Forum, 2006. **522-523**: p. 563-570.
2. Pettersson, C., *The role of KCl in the high temperature corrosion of alloy Sanicro 28*, in *Department of Inorganic Chemistry*. 2003, Gothenburg University: Gothenburg. p. 42.
3. Spiegel, M., *Salt melt induced corrosion of metallic materials in waste incineration plants*. Materials and Corrosion-Werkstoffe Und Korrosion, 1999. **50**(7): p. 373-393.
4. Spiegel, M., A. Zahs, and H.J. Grabke, *Fundamental aspects of chlorine induced corrosion in power plants*. Materials at High Temperatures, 2003. **20**(2): p. 153-159.
5. Grabke, H.J., E. Reese, and M. Spiegel, *The effects of chlorides, hydrogen chloride, and sulfur dioxide in the oxidation of steels below deposits*. Corrosion Science, 1995. **37**(7): p. 1023-43.
6. Montgomery, M., A. Karlsson, and O.H. Larsen, *Field test corrosion experiments in Denmark with biomass fuels. Part 1: straw-firing*. Materials and Corrosion, 2002. **53**(2): p. 121-131.
7. Nielsen, H.P., F.J. Frandsen, and K. Dam-Johansen, *Lab-Scale Investigations of High-Temperature Corrosion Phenomena in Straw-Fired Boilers*. Energy & Fuels, 1999. **13**(6): p. 1114-1121.
8. Pettersson, J., et al., *KCl induced corrosion of a 304-type austenitic stainless steel at 600 degrees C; The role of potassium*. Oxidation of Metals, 2005. **64**(1-2): p. 23-41.



9. Pettersson, C., et al., *KCl-induced high temperature corrosion of the austenitic Fe-Cr-Ni alloys 304L and Sanicro 28 at 600 degrees C*. Corrosion Science, 2006. **48**(6): p. 1368-1378.
10. Karlsson, S., Pettersson, J., Svensson, J. -E., Johansson, L. -G., *Alkali Induced High Temperature Corrosion - The Influence of Different Chlorine Containing Salts*. Submitted to "Oxidation of Metals".
11. Pettersson, J., N.Folkesson., Svensson, J. -E., Johansson, L. -G., *The Effects of KCl, K<sub>2</sub>SO<sub>4</sub> and K<sub>2</sub>CO<sub>3</sub> on the High Temperature Corrosion of a 304-type Austenitic Stainless Steel*. Accepted by Oxidation of Metals.
12. Pettersson, C., Johansson, L.-G., Svensson, J.-E., *The influence of small amounts of KCl(s) on initial stages of the corrosion of alloy Sanicro 28 at 600°C*. Submitted to oxidation of metals.
13. Asteman, H., J.E. Svensson, and L.G. Johansson, *Evidence for chromium evaporation influencing the oxidation of 304L: The effect of temperature and flow rate*. Oxidation of Metals, 2002. **57**(3-4): p. 193-216.
14. Pettersson, J., Asteman, H., Svensson, J. -E., Johansson, L. -G., *KCl Induced Corrosion of a 304-type Austenitic Stainless Steel at 600°C; The Role of Potassium*. Oxidation of Metals, 2005. **64**(1 - 2): p. 23-41.
15. Pettersson, C., Pettersson, J., Asteman, H., Svensson, J. E., Johansson, L. G., *KCl-induced high temperature corrosion of the austenitic Fe-Cr-Ni alloys 304L and Sanicro 28 at 600°C*. Corrosion Science, 2006. **48**(6): p. 1368-1378.
16. Barin, I., *Thermodynamic Data of Pure Substances*. Third Edition ed. 1995.
17. Jonsson, T., et al., *The Influence of KCl on the Corrosion of an Austenitic Stainless Steel (304L) in Oxidizing Humid Conditions at 600 degrees C: A Microstructural Study*. Oxidation of Metals, 2009. **72**(3-4): p. 213-239.
18. N. Folkesson, T.J., M. Halvarsson, L-G. Johansson and J.-E Svensson, *The Influence of Small amounts of KCl(s) on the High Temperature Corrosion of Fe-2.25Cr-1Mo Steel at 400° and 500°C*. Materials and Corrosion 2010. **61**.